PHYSICAL REVIEW B **92**, 220421(R) (2015)

Dynamical process of skyrmion-helical magnetic transformation of the chiral-lattice magnet FeGe probed by small-angle resonant soft x-ray scattering

Y. Yamasaki,[1,2] D. Morikawa,[2] T. Honda,[3] H. Nakao,[3] Y. Murakami,[3] N. Kanazawa,[1] M. Kawasaki,[1,2] T. Arima,[2,4] and Y. Tokura[1,2]

[1]*Department of Applied Physics and Quantum-Phase Electronics Center (QPEC), University of Tokyo, Tokyo 113-8656, Japan*

[2]*RIKEN Center for Emergent Matter Science (CEMS), Wako 351-0198, Japan*

[3]*Condensed Matter Research Center and Photon Factory, Institute of Materials Structure Science, High Energy Accelerator Research Organization, Tsukuba 305-0801, Japan*

[4]*Department of Advanced Materials Science, University of Tokyo, Kashiwa 277-8561, Japan*

(Received 13 May 2015; revised manuscript received 24 November 2015; published 28 December 2015)

Small-angle soft x-ray scattering in resonance with Fe L absorption edge has been investigated for helical magnetic order and magnetic skyrmion crystal (SkX) in B20-type cubic FeGe. Transformation of magnetic structures among helical, conical, SkX, and field-polarized spin-collinear forms is observed with the application of a magnetic field parallel to the incident soft x-ray. The resonant soft x-ray scattering with high $\boldsymbol{q}$-resolution revealed a transient dynamics of SkX, such as rotation of SkX and variation of the SkX lattice constant, upon the change of magnetic field.

DOI: 10.1103/PhysRevB.92.220421 PACS number(s): 75.75.−c, 61.05.cf

A topological spin texture, known as a magnetic skyrmion, is induced by the Dzyaloshinskii-Moriya interaction due to the breaking of inversion symmetry of crystal lattice in a noncentrosymmetric ferromagnet [1–3]. The formation of skyrmion crystal (SkX), i.e., the triangular lattice of skyrmions, has been observed for bulk crystals and thin films of chiral-lattice ferromagnetic alloys by small-angle neutron scattering (SANS) and Lorentz transmission electron microscopy [4,5]. The topologically protected nanoscale skyrmions have high potential for spintronic applications [6–9]. A fast melting of the SkX is anticipated to occur by intensive excitation of skyrmion collective modes [10], such as breathing and rotation modes [11,12], which will be an important function for a high-speed spintronics device. Development of a time-resolved probe of SkX is strongly required for elucidating the dynamical response of SkX [13].

In this Rapid Communication, we report on the investigation of the helical and SkX magnetic structures by resonant soft x-ray scattering (RSXS), a useful method to detect the magnetic order in 3d transition-metal compounds with use of core excitations from the transition-metal 2p to the 3d states. Sixfold magnetic diffraction from the SkX was observed around a lattice Bragg spot of (001) at Cu L edge for Cu_2OSeO_3 [14]. However, since it is applicable only to the materials where the Bragg peak of lattice is observable by long-wavelength soft x-rays, choice of material is restricted for this method. In the present experiment, we employed a small-angle RSXS method to measure magnetic reflections at around the direct beam, which would be applicable to versatile materials hosting SkX. In addition, the coherent soft x-ray scattering is capable of reconstructing a real-space image of magnetic moment distribution [15] and may also offer the opportunity for time-resolved measurements of fast SkX dynamics [13].

Small-angle RSXS at Fe L absorption edge was performed in a single-crystal plate of FeGe, which is a B20-type cubic alloy with noncentrosymmetric crystal structure (space group $P2_13$) and shows helical magnetic order below 278.7 K with a magnetic modulation period of ∼70 nm [16]. The SkX phase shows up with an application of magnetic field and extends over a wider temperature and magnetic field region in a thinner sample [17]. Since the attenuation length of soft x-ray at Fe L_3 edge (∼707 eV) in FeGe is less than 100 nm, a thin plate sample has to be prepared for observation of transmitted small-angle RSXS.

A single crystal of B20-type FeGe was grown by chemical vapor transport with use of I_2 as transport agent. A thin plate with a thickness less than 200 nm for small-angle RSXS observation was prepared by the focused ion beam thinning method. The sample was affixed with tungsten contacts on a Si substrate with a hole of 4 μm in diameter, as shown in the inset of Fig. 1(a). A gold thin plate, on which a pinhole with a diameter of 0.5 μm was drilled, was placed adjacent to the FeGe thin plate and was used as a reference hole to measure the holographic image [15].

Small-angle RSXS measurements were carried out at a soft x-ray beamline BL-16A, Photon Factory, KEK, Japan, which is equipped with a high vacuum chamber with a background pressure of 1×10^{-8} Torr. A schematic of the experimental geometry is displayed in Fig. 1(a). The incident soft x rays were tuned to be circularly polarized. An in-vacuum CCD camera (512 × 512 pixel, Princeton Instruments), positioned downstream from the sample, was used to record the RSXS. Magnetic field up to 0.5 T was applied parallel to the incident soft x ray by a Helmholtz coil. The temperature was controlled with a He-flow-type refrigerator.

Figure 1(b) shows the x-ray absorption spectrum (XAS) in a transmission mode and the small-angle RSXS spectrum for the helical (proper screw) magnetic structure at 260 K and 0 T. The absorption peaks at around 708 and 720 eV are assigned to the Fe $L_3(2p_{3/2} \rightarrow 3d)$ and $L_2(2p_{1/2} \rightarrow 3d)$ edges, respectively. The spectral peaks of RSXS due to the helical magnetic structure were observed at 707 eV (L_3) and 719 eV (L_2). Figures 1(c)–1(h) show the schematics of magnetic structure and the CCD images of RSXS for helical at 0 T [(c) and (d)], SkX at 0.1 T [(e) and (f)], and field-polarized spin-collinear (ferromagnetic) structures at 0.4 T [(g) and (h)], respectively. The x-ray beam through the reference

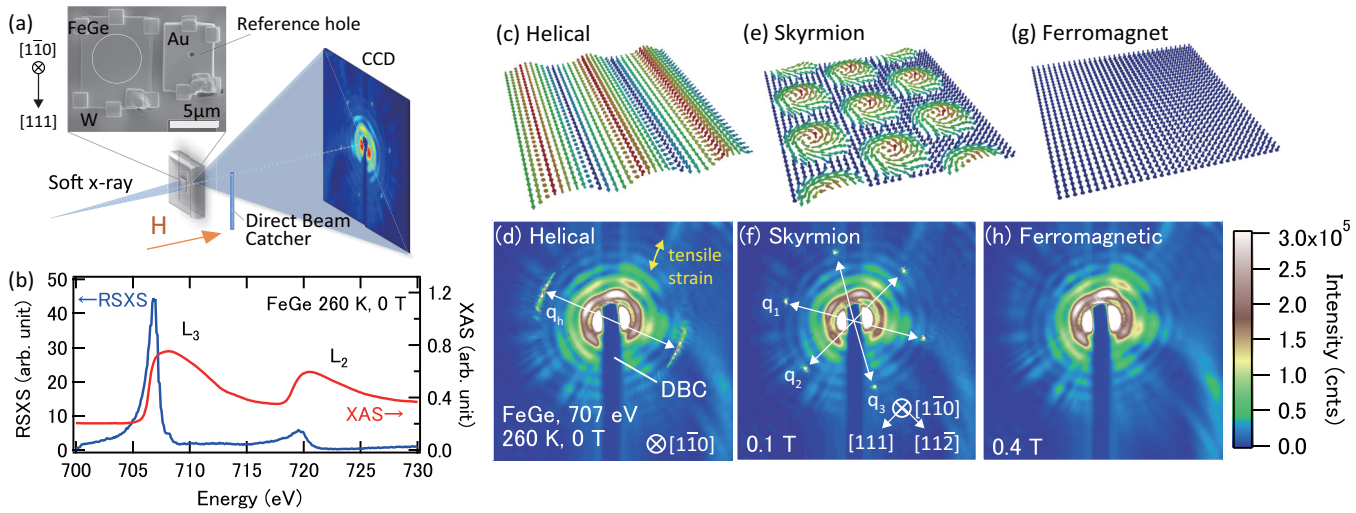

FIG. 1. (Color online) (a) Schematic of small-angle resonant x-ray scattering and picture of sample. (b) Energy spectra for XAS and RSXS. Observed CCD images of small-angle RSXS and corresponding schematic illustrations of magnetic structures for helical [(d) and (c)], skyrmion crystal [(f) and (e)], and field-polarized spin-collinear (ferromagnetic) phase [(h) and (g)]. The yellow arrow in Fig. 1(d) indicates the estimated direction of tensile strain from the substrate.

hole causes concentric circle diffraction images around the direct beam; its pitch corresponds to the reciprocal of pinhole size. Twofold symmetric arclike magnetic peaks ($\boldsymbol{q} = \pm\boldsymbol{q_h}$) observed in Fig. 1(d) come from the helical magnetic ordering. An application of magnetic field of 0.1 T turns the diffraction to the sixfold pattern ($\boldsymbol{q} = \pm\boldsymbol{q_1}, \pm\boldsymbol{q_2}, \pm\boldsymbol{q_3}$) characteristic of the formation of SkX [Fig. 1(f)]. The SkX phase was observed to subsist up to 0.15 T perhaps due to the thin plate thickness [17,18]. As a higher magnetic field of 0.4 T is applied, the magnetic structure becomes a field-polarized spin-collinear structure and the small-angle magnetic scattering totally vanishes [Fig. 1(h)]. A similar transition from the helical to the collinear phase by way of the SkX phase with increasing magnetic field was confirmed in a wide temperature range from 250 K up to 280 K while squeezing the SkX phase region with increasing temperature. Hereafter, we focus on the transition dynamics of the SkX at a fixed temperature of 260 K.

Figure 2(a) shows azimuthal angle (ϕ) dependence of intensity integrated along the radial $\boldsymbol{q}$ direction in the range of $7.5 \times 10^{-2} \leqslant |\boldsymbol{q}| \leqslant 10.5 \times 10^{-2}$ nm^{-1} for helical order (0 T) and SkX (0.1 T). Two broad magnetic peaks show up at $\phi = 0$ and π in the helical phase at 0 T, while six pronounced sharp magnetic diffraction spots are observed every 60° in the SkX phase at 0.1 T. Figure 2(b) shows the magnetic diffraction intensities as a function of $q(=|\boldsymbol{q}|)$ for 0 T (helical order) and 0.1 T (SkX). Magnetic diffraction appears at $|\boldsymbol{q_h}| = 9.4 \times 10^{-2}$ nm^{-1} for the helical order and at $|\boldsymbol{q_1}| = 8.6 \times 10^{-2}$ nm^{-1} for the SkX, which correspond to the helical magnetic wavelength of $\lambda_h = 68$ nm and to the distance between nearest neighboring skyrmions of 83 nm, respectively. Although it has been reported in the SANS study on FeGe that the magnitudes of $\boldsymbol{q}$ vector are coincident between the helical order and the SkX [18], the present study revealed the difference, i.e., $|\boldsymbol{q_h}| > |\boldsymbol{q_1}|$, due to the high $\boldsymbol{q}$-resolution of RSXS (the transverse q resolution was estimated to be 0.003 nm^{-1}).

The magnitude of $\boldsymbol{q}$ vector of SkX depends on its direction, i.e., $|\boldsymbol{q}_1| \neq |\boldsymbol{q}_2|$ [Fig. 1(f)] as shown in Fig. 2(b), indicating the homogeneous deformation of the triangular lattice of SkX. These magnetic peaks from the SkX trace an ellipse with a ratio of the minor radius to the major radius of 0.96 and the major axis of the ellipse nearly coincides with the direction of $\boldsymbol{q_h}$. These phenomena can be elucidated by strain from the substrate; the tensile strain favors a larger spacing of SkX along the strain direction and $\boldsymbol{q_h}$ perpendicular to the strain direction [19]. In the present experiment, we can estimate from the preceding study [19] that the uniaxial strain of 0.05% is induced along $\phi = \pm 90°$ due to the asymmetric position of tungsten contacts [see the inset of Fig. 1(a)]. In the SkX phase, as shown in Fig. 2(c), a second-order magnetic reflection ($\boldsymbol{2q}$) is also discerned with an intensity weaker than the primary one ($\boldsymbol{q}$) by two orders of magnitude. The $2\boldsymbol{q}$ reflection can be assigned to a second-order reflection but not to double scattering, because it is not observed in the helical phase. The presence of such a higher harmonic order scattering indicates the deviation of the actual magnetic configuration from a pure sine curve, and thus the deviation of the SkX from a simple sine wave triple-$\boldsymbol{q}$ configuration.

In the present experimental setup, the interference between the resonant soft x-ray scattering and the diffraction from the reference hole was too weak to reconstruct the real image of magnetic moment distribution via a Fourier transformation of holographic image. This is partly because the intensity of magnetic scattering was about ten times larger than that of the reference hole, as shown in Fig. 2(c). Hereafter, we focus on the dynamical behavior of magnetic scattering peaks. The detailed investigations on imaging of magnetic moment distribution by coherent soft x ray will be described elsewhere.

Figure 3 shows (a) the intensity of magnetic diffraction, (b) the contour plot for magnitude of $\boldsymbol{q}$ vector ($q = |\boldsymbol{q_h}|, |\boldsymbol{q_1}|$), and (c) the azimuthal angle ϕ in the helical, conical, and SkX phases as a function of magnetic field. Since the magnetic scattering intensity becomes its maximum at 0.1 T, the data are depicted in the region between 0 and 0.1 T. In the present measurement, the magnetic field is gradually varied with a sweep rate less than 0.1 T/min. In the helical phase between

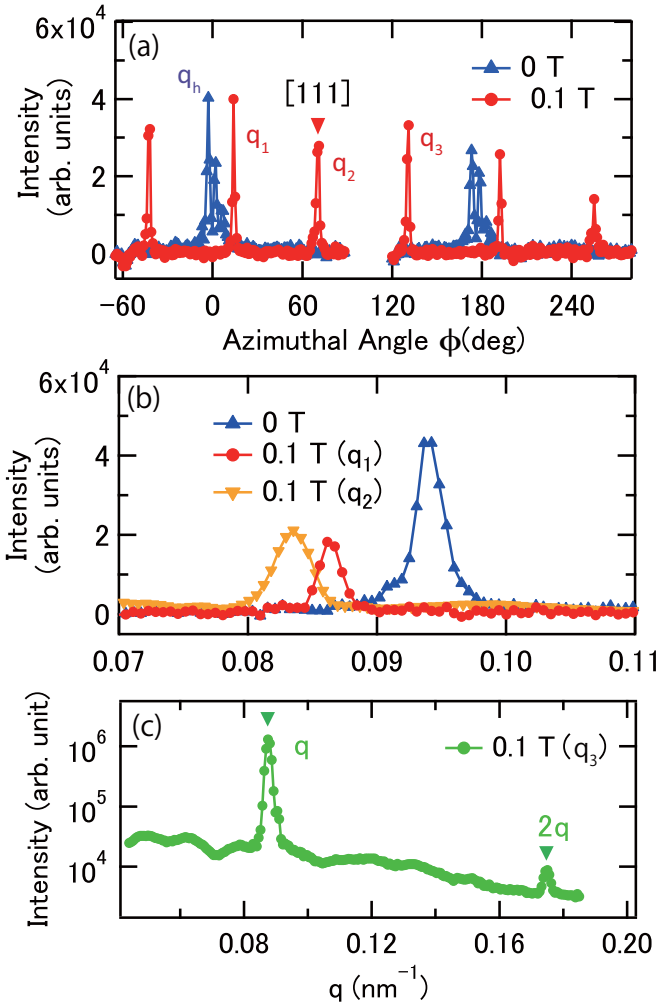

FIG. 2. (Color online) (a) Azimuthal angle ϕ and (b) $q(=|\boldsymbol{q}|)$ dependence of small-angle RSXS intensities for the helical and the SkX phases. The origin of azimuthal angle ($\phi = 0$) is taken at the position of the diffraction of the helical state [Fig. 1(d)]. See also Fig. 1(f) for the definition of $\boldsymbol{q}$ vector. (c) q dependence of small-angle RSXS intensity from the SkX along the $\boldsymbol{q}_3$ including high-q region. A periodic modulation of the background intensity is due to the scattering from the reference hole.

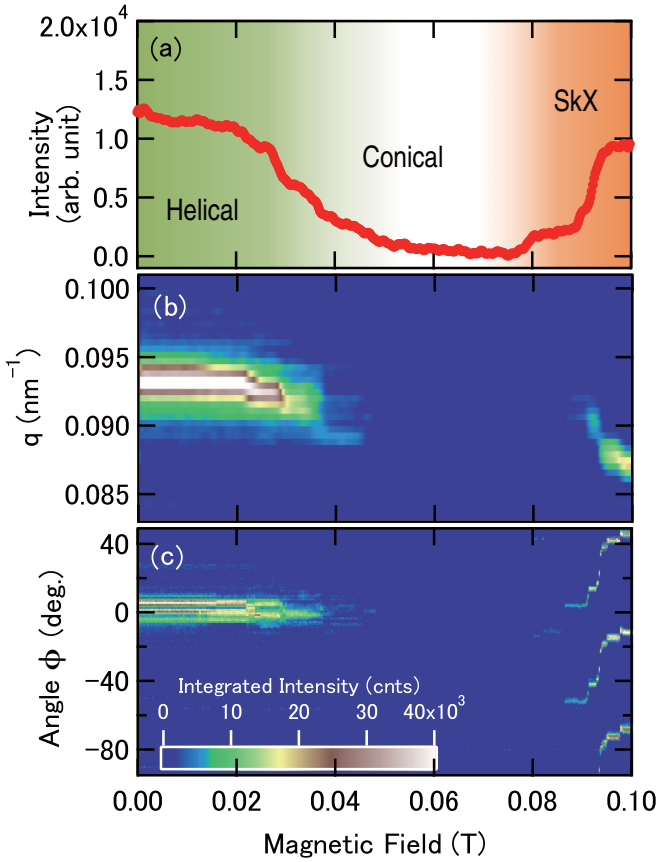

FIG. 3. (Color online) Magnetic field dependence of (a) scattering intensity integrated in the range of $0.075 \leqslant |\boldsymbol{q}| \leqslant 0.105$ and $120^\circ \leqslant \phi \leqslant 300^\circ$, (b) the contour plot for $q = |\boldsymbol{q}_h|, |\boldsymbol{q}_1|$, and (c) the contour plot for ϕ integrated in $0.075 \leqslant q \leqslant 0.105$.

0 and 0.04 T, the intensity and q decrease as the magnetic field is increased, while the direction of $\boldsymbol{q}$ keeps its initial position. No in-plane magnetic scattering is discerned between 0.04 and 0.08 T, where the magnetic modulation is likely to be aligned parallel to the normal direction of the thin plate sample and to form the vertical conical magnetic state. Above 0.08 T, three pairs of sharp magnetic diffractions emerge from the SkX, and then q decreases in magnitude and rotates as increasing magnetic field. Such a successive rotation of SkX with varying magnetic field has not been observed so far for SkX materials, while a 30° rotation of the SkX across the two SkX phases has been reported for Cu_2OSeO_3 [20]. The azimuthal angle of the SkX does not change above 0.1 T and the scattering intensity from the SkX disappears at around 0.13 T (not shown). However, whether it goes directly to the field-polarized spin-collinear phase or by way of the conical phase cannot be distinguished in the present experimental setup.

We measured magnetic scattering peaks with repeating magnetic field cycles between 0 and 0.1 T at 20-s intervals to survey the dynamics upon the transformation between the helical and SkX magnetic structures. Figures 4(a)–4(c) show the magnetic-field strength, ϕ, and $q(=|\boldsymbol{q}|)$ as a function of time. First, the magnetic scattering from the helical magnetic structure is observed at $\phi = 0^\circ$ in a time span between 0 and 20 s with 0 T. Then, the magnetic diffraction from the SkX shows up at $\phi \sim -20^\circ$ and $\phi \sim -80^\circ$ from 20 to 40 s with applied magnetic field of 0.1 T. After the helical phase again shows up between 40 and 60 s with 0 T, magnetic reflections are observed at $\phi \sim 20^\circ$ and $\phi \sim -40^\circ$ between 60 and 80 s at 0.1 T. These behaviors show that there are two types of SkX orientations, with $\boldsymbol{q}$ vectors pointing at $\phi = \frac{n\pi}{3} - 20^\circ$ and $\phi = \frac{n\pi}{3} + 20^\circ$ (n = integer), respectively. Hereafter, we refer to them as SkX I and II. In subsequent field applications, the SkX I appears between 100 and 120 s and between 140 and 160 s, while the SkX II does between 180 and 200 s, indicating that the SkX I or II shows up in a random manner. It is likely that there are two degenerate pinning regimes for SkX orientations.

While one of the three $\boldsymbol{q}$ vectors of SkX in a magnetic field parallel to the $[1\bar{1}0]$ is usually pinned along a [110] direction in B20-type crystals [21,22], neither of the present two SkXs has a $\boldsymbol{q}$ vector pointing along the [110] direction.

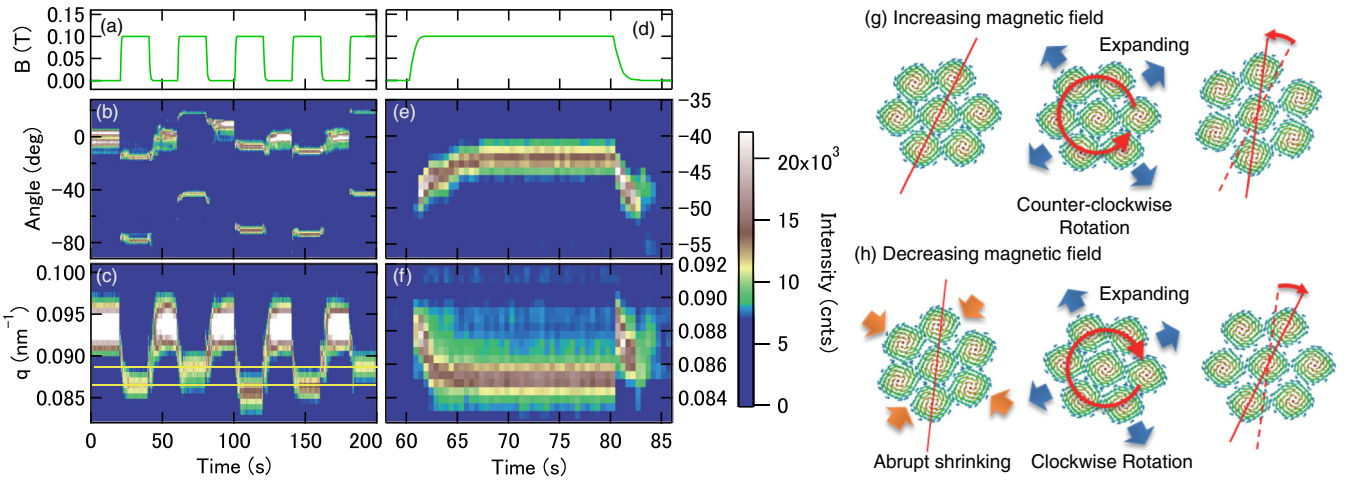

FIG. 4. (Color online) Temporal change of applied magnetic field [(a) and (d)], the azimuthal angle ϕ [(b) and (e)], and the magnitude of $\boldsymbol{q}$ vector ($q = |\boldsymbol{q}|$) [(c) and (f)] of magnetic scattering from helical and SkX magnetic structures. The schematic pictures of transient variation in SkX structure (g) from helical to SkX as increasing magnetic field and (h) from the SkX to helical magnetic structure as decreasing magnetic field.

The discrepancy can be elucidated by the residual tensile strain from the substrate, which may modulate the anisotropy term and tilt the stable orientation of the SkX. The slight difference in q values between SkX I and II, as shown in Fig. 4(c), can be also elucidated by the difference in the strain effect.

Figures 4(d)–4(f) show magnified views of q and ϕ behaviors in the range from 20 to 40 s. Upon the transformation from helical to SkX phase with applying magnetic field, the rotation of SkX occurs concurrently with expanding lattice constant (decreasing q value) of SkX [Fig. 4(g)]. Upon switching off the magnetic field, the SkX q value abruptly increases and then turns to decrease in a few seconds, and finally the SkX vanishes abruptly, transforming to the helical phase. Namely, abrupt shrinking of SkX occurs just after switching off the magnetic field and subsequent rotation and expansion of SkX occur [Fig. 4(h)]. These results suggest that the expansion of lattice constant of SkX should be always accompanied by a rotation of SkX.

The present study has revealed that the SkX rotates while changing lattice constant of SkX upon switching on and off the applied magnetic field. Rotational motions in SkX have been observed so far as induced by an electric field [9], temperature gradient [23,24], pulse magnetic field [13], or irradiating soft x-ray [14]. In the present case, some driving force to leap over the potential barrier between these two pinning regimes of the SkX I and II is required to rotate the SkX. Since the rotation of SkX always occurs during magnetic field change, one may think that an eddy current induced on the sample due to the sweeping magnetic field would play some role. However, it is estimated to be far smaller than the threshold of electric current for the SkX motion [8,23]. The rotational motion of SkX may be caused by a combination of magnetic field change and the effect of soft x-ray irradiation, i.e., photoinduced spatial gradient of temperature and/or spin excitations. The expansion and shrinkage of the SkX lattice constant should be strongly coupled with the rotating motion of the SkX. The shrinking of the SkX may be forming microdomains or clusters of skyrmions and then the rotation of SkX may become possible within the individual domains, resulting in the apparent rotation of the whole SkX. Such a loss of coherence in SkX may be related to the broadening of the magnetic peak along the radial $\boldsymbol{q}$ direction, as seen in Fig. 4(f).

In conclusion, the helical magnetic structure and the SkX in FeGe are observed by the small-angle magnetic scattering with soft x-ray resonant with Fe L edge. The high-$\boldsymbol{q}$-resolution magnetic reflections reveal the difference in the q value between the helical order and the SkX, and also the sensitive deformation of SkX due to the strain from the substrate. Moreover, the small-angle RSXS confirms the transient motion of the SkX upon the change of magnetic field, such as the expansion of lattice constant and concurrent rotation of the SkX. The measurement with use of coherent and pulse soft x-ray will reveal further dynamics of skyrmions toward their spintronics application.

The authors are grateful to K. Shibata, J. Okamoto, T. Sudayama, K. Amemiya, M. Sakamaki, Masato Kubota, and Masashi Kubota for their enlightening discussions. This work was supported by Grants-in-Aid for Scientific Research (Grants No. 21224008, No. 22740243, No. 24224009(S), No. 25286090, and No. 15H05456) from the Japan Society for the Promotion of Science and by the Japan Society for the Promotion of Science through the Funding Program for World-Leading Innovative R&D on Science and Technology (FIRST Program). The synchrotron radiation experiments were performed in Photon Factory with the approval of Photon Factory Program Advisory Committee (Proposals No. 2009S2-008, No. 2012S2-005, No. 2010G086, No. 2011G597, No. 2013G733, and No. 2015S2-007).

[1] T. H. R. Skyrme, Nucl. Phys. **31**, 556 (1962).
[2] U. Rößler, A. Bogdanov, and C. Pfleiderer, Nature (London) **442**, 797 (2006).
[3] N. Nagaosa and Y. Tokura, Nat. Nanotechnol. **8**, 899 (2013).
[4] S. Mühlbauer, B. Binz, F. Jonietz, C. Pfleiderer, A. Rosch, A. Neubauer, R. Georgii, and P. Böni, Science **323**, 915 (2009).
[5] X. Yu, Y. Onose, N. Kanazawa, J. Park, J. Han, Y. Matsui, N. Nagaosa, and Y. Tokura, Nature (London) **465**, 901 (2010).
[6] F. Jonietz, S. Mühlbauer, C. Pfleiderer, A. Neubauer, W. Münzer, A. Bauer, T. Adams, R. Georgii, P. Böni, R. Duine *et al.*, Science **330**, 1648 (2010).
[7] J. Iwasaki, M. Mochizuki, and N. Nagaosa, Nat. Nanotechnol. **8**, 742 (2013).
[8] T. Schulz, R. Ritz, A. Bauer, M. Halder, M. Wagner, C. Franz, C. Pfleiderer, K. Everschor, M. Garst, and A. Rosch, Nat. Phys. **8**, 301 (2012).
[9] J. White, K. Prša, P. Huang, A. Omrani, I. Živković, M. Bartkowiak, H. Berger, A. Magrez, J. Gavilano, G. Nagy *et al.*, Phys. Rev. Lett. **113**, 107203 (2014).
[10] M. Mochizuki, Phys. Rev. Lett. **108**, 017601 (2012).
[11] Y. Onose, Y. Okamura, S. Seki, S. Ishiwata, and Y. Tokura, Phys. Rev. Lett. **109**, 037603 (2012).
[12] T. Schwarze, J. Waizner, M. Garst, A. Bauer, I. Stasinopoulos, H. Berger, C. Pfleiderer, and D. Grundler, Nat. Mater. **14**, 478 (2015).
[13] F. Büttner, C. Moutafis, M. Schneider, B. Krüger, C. Günther, J. Geilhufe, C. v. K. Schmising, J. Mohanty, B. Pfau, S. Schaffert *et al.*, Nat. Phys. **11**, 225 (2015).
[14] M. Langner, S. Roy, S. Mishra, J. Lee, X. Shi, M. Hossain, Y.-D. Chuang, S. Seki, Y. Tokura, S. Kevan *et al.*, Phys. Rev. Lett. **112**, 167202 (2014).
[15] S. Eisebitt, J. Lüning, W. Schlotter, M. Lörgen, O. Hellwig, W. Eberhardt, and J. Stöhr, Nature (London) **432**, 885 (2004).
[16] B. Lebech, J. Bernhard, and T. Freltoft, J. Phys.: Condens. Matter **1**, 6105 (1989).
[17] X. Z. Yu, N. Kanazawa, Y. Onose, K. Kimoto, W. Z. Zhang, S. Ishiwata, Y. Matsui, and Y. Tokura, Nat. Mater. **10**, 106 (2011).
[18] E. Moskvin, S. Grigoriev, V. Dyadkin, H. Eckerlebe, M. Baenitz, M. Schmidt, and H. Wilhelm, Phys. Rev. Lett. **110**, 077207 (2013).
[19] K. Shibata, J. Iwasaki, N. Kanazawa, S. Aizawa, T. Tanigaki, M. Shirai, T. Nakajima, M. Kubota, M. Kawasaki, H. S. Park *et al.*, Nat. Nanotechnol. **10**, 589 (2015).
[20] S. Seki, J.-H. Kim, D. S. Inosov, R. Georgii, B. Keimer, S. Ishiwata, and Y. Tokura, Phys. Rev. B **85**, 220406 (2012).
[21] W. Münzer, A. Neubauer, T. Adams, S. Mühlbauer, C. Franz, F. Jonietz, R. Georgii, P. Böni, B. Pedersen, M. Schmidt, A. Rosch, and C. Pfleiderer, Phys. Rev. B **81**, 041203(R) (2010).
[22] T. Adams, S. Mühlbauer, A. Neubauer, W. Münzer, F. Jonietz, R. Georgii, B. Pedersen, P. Böni, A. Rosch, and C. Pfleiderer, J. Phys: Conf. Ser. **200**, 032001 (2010).
[23] M. Mochizuki, X. Yu, S. Seki, N. Kanazawa, W. Koshibae, J. Zang, M. Mostovoy, Y. Tokura, and N. Nagaosa, Nat. Mater. **13**, 241 (2014).
[24] K. Everschor, M. Garst, B. Binz, F. Jonietz, S. Mühlbauer, C. Pfleiderer, and A. Rosch, Phys. Rev. B **86**, 054432 (2012).